Supporting Information

Wenz et al. 10.1073/pnas.0911570106

SI Text

Blood Work. Blood was withdrawn from deeply anesthesized animals by cardiac puncture, serum was obtained, and the levels of creatine kinase, lactate, and triglycerides were determined by the Comparative Pathology Laboratory at the University of Miami, Miller School of Medicine.

DEXA Scans. Fat and lean body mass as well as bone mineral density were assessed by DEXA scan using the Lunar Piximus densitometer according to manufacturer's recommendations.

Histochemistry and Immunohistochemistry. Muscle tissue was frozen in isopentane liquid nitrogen. Cross-sections (8-μm) were stained for COX, SDH, and combined activities. Muscle sections were also stained with H&E to assess muscle fiber area and general morphology (1). Vascular structure in the muscle was assessed by the alkaline phosphatase activity of the endothelial cells of the blood capillaries (2). Collagen was stained by the Picrosirius Red method (3). For immunohistochemistry, muscle sections were treated with 0.5% Triton X-100 in PBS for 30 min and washed in PBS for 30 min before the addition of an anti-cleaved caspase 3 and anti-8-OH-guanosine following labeling with an Alexa fluor 488-conjugated secondary antibody (Molecular Probes).

Isolation of Mitochondria and Measurement of OXPHOS Complex Activity. Mitochondrial preparations were obtained as described and stored at −80 °C until needed. Muscle homogenates were prepared by homogenizing a snap-frozen muscle piece (≈50 mg) in 500 μL 10 mM HEPES, pH 7.4, 0.5 mM EDTA, 0.5 mM EGTA, 250 mM sucrose, and used immediately. Enzyme activities were determined spectrophotometrically as described in ref. 4. Protein concentrations were estimated by the method of Bradford using BSA as a standard.

Western Blots. Western blot analysis was performed as described in ref. 4. Antibodies against different subunits of the oxidative phosphorylation complexes (ND39, SDH, COXI, ATPaseβ), SOD2, HSP70, and VDAC were obtained from Molecular Probes, and an antibody against tubulin was obtained from Chemicon International. Antibodies against p65-NFκB, LC3, 20S proteasome, Bax, Bcl2, ubiquitin, Akt/pAkt, and mTOR/pmTOR were obtained from Cell Signaling Technology.

Real-Time Quantitative PCR. Total RNA was extracted from snap-frozen muscle by TRIzol (Life Technologies). cDNA was synthesized using the SuperScript First Strand kit (Invitrogen). Quantitative real-time PCRs were performed on the cDNAs in the presence of fluorescent dye (SYBR Green; Qiagen). All results are expressed as means ± SEM. The results were normalized for comparison by measuring β-actin mRNA levels in each sample.

Analysis of the NMJ. AChE enzyme activity and oligomeric forms were assessed as described in ref. 5. Briefly, hind limb muscles were homogenized in 10 volumes of extraction buffer consisting of 20 mM sodium borate buffer, pH 9.0, 1 M NaCl, 1.0% Triton X-100, 10 mM EDTA, and protease inhibitors. Aliquots were analyzed by velocity sedimentation on 5–20% sucrose gradients, and the fractions were assayed for AChE activity using the colorimetric Ellman assay (6). For quantitative analysis of the NMJs, mouse thigh muscles were labeled with Alexa-555 α-Btx and Alexa-488 Fasciculin2, and digital images were taken at two wavelengths appropriate to each fluorophore using a Princeton Instruments Micromax camera mounted on a Leica DMR-A microscope. Images were captured using Slidebook 4.0 software and measured using a calibrated optical micrometer. For analysis of AChE and AChR, the images were captured using identical exposure parameters and the fluorescence intensity at each wavelength expressed as relative units.

Catalase Activity Assay. The Amplex Red Catalase Assay kit (Molecular Probes) was used to measure catalase activity in muscle mitochondria.

Detection of Oxidized Proteins. Detection and quantification of carbonylated proteins were carried out using the Oxyblot Protein Oxidation kit (Chemicon International) according to the manufacturer's recommendations.

ELISA for TNFα and IL-6. The TNFα and IL-6 ELISA kit from eBioscience was used according to manufacturer's recommendation. Serial dilations of serum and cleared tissue homogenate were used.

Cell Death ELISA for Determination of the Apoptotic Index. The extent of apoptotic DNA fragmentation (apoptotic index) was quantified by measuring the amount of cytosolic mono- and oligonucleosomes (180-bp nucleotides or multiples) using an ELISA kit (Cell Death Detection ELISA; Roche Diagnostics) following the manufacturer's instructions. Serial dilutions of cytosolic extracts were used.

Glucose and Insulin Tolerance Test. Following an overnight fast, mice were administered glucose (2 g/kg i.p.) by oral gavage, and blood samples for glucose and insulin determination were collected from the tail vein at the indicated times. Insulin tolerance was assessed after a 6 h fast by administration of human insulin (1 U/kg i.p.) and blood glucose monitoring. Glycemia was assessed using a Precision Xtra (MediSense) glucometer.

1. Sciacco M, Bonilla E (1996) Cytochemistry and immunocytochemistry of mitochondria in tissue sections. *Methods Enzymol* 264:509–521.
2. Hansen-Smith FM, Blackwell LH, Joswiak GR (1992) Expression of muscle capillary alkaline phosphatase is affected by hypoxia. *J Appl Physiol* 73:776–780.
3. Whittaker P, Kloner RA, Boughner DR, Pickering JG (1994) Quantitative assessment of myocardial collagen with picrosirius red staining and circularly polarized light. *Basic Res Cardiol* 89:397–410.
4. Diaz F, Thomas CK, Garcia S, Hernandez D, Moraes CT (2005) Mice lacking COX10 in skeletal muscle recapitulate the phenotype of progressive mitochondrial myopathies associated with cytochrome c oxidase deficiency. *Hum Mol Genet* 14:2737–2748.
5. Rossi SG, Rotundo RL (1993) Localization of ''non-extractable'' acetylcholinesterase to the vertebrate neuromuscular junction. *J Biol Chem* 268:19152–19159.
6. Ellman GL, Courtney KD, Andres V, Jr, Feather-Stone RM (1961) A new and rapid colorimetric determination of acetylcholinesterase activity. *Biochem Pharmacol* 7:88–95.

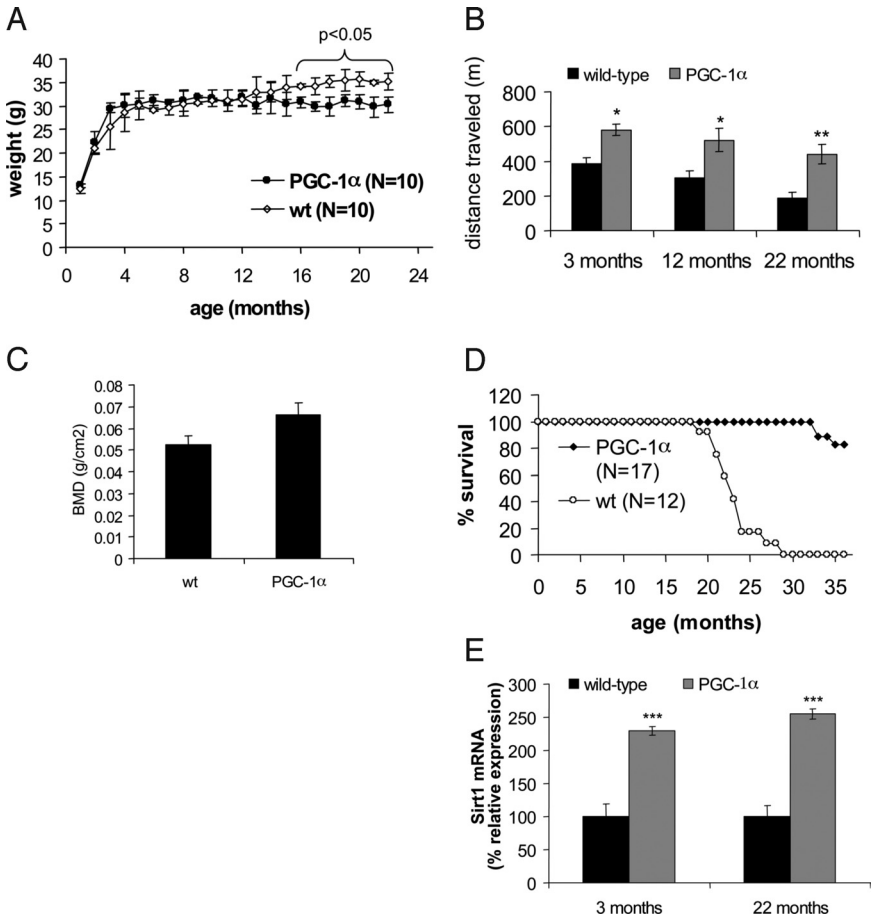

Fig. S1. Mice with increased PGC-1α in muscle has a younger phenotype. (*A*) Weight development ($n = 10$ for each group, and bars represent SD). (*B*) Endurance performance test (distance traveled) at 3 and 22 months of age ($n = 9$ for each mouse group, and bars represent SD). *, $P < 0.001$. (*C*) Bone mineral density for 22-month-old wild-type and PGC-1α animals as determined by DEXA scans ($n = 6$ for each group, and bars represent SD). *, $P > 0.05$. (*D*) Survival curve for wild-type and PGC-1α animals. (*E*) Relative expression of Sirt1 in 3- and 22-month-old wild-type and PGC-1α animals ($n = 3$ for each group, and bars represent SD).

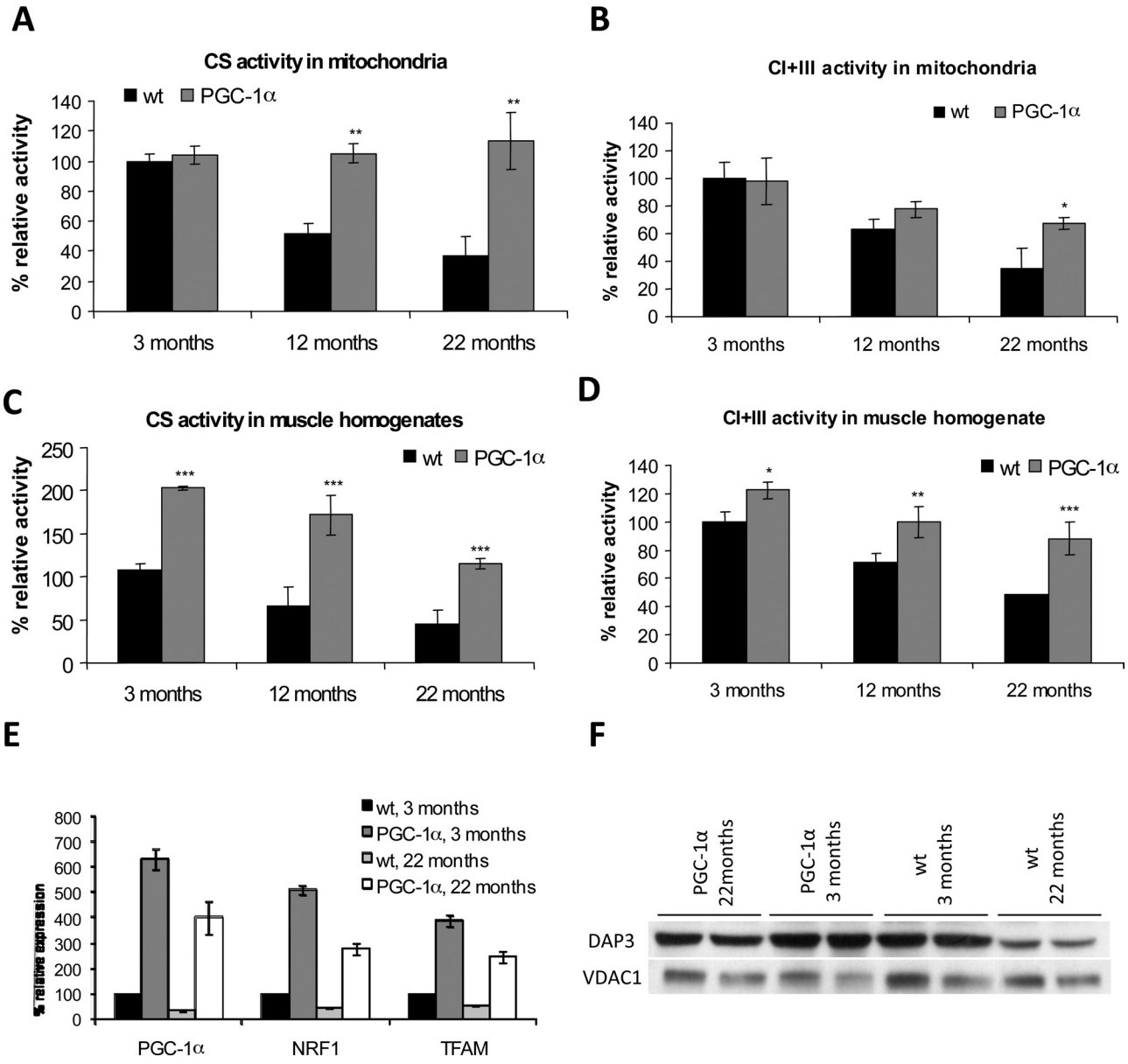

Fig. S2. Mitochondrial enzymes and components are increased in muscle with increased PGC-1α. (*A–D*) Activities for CS and CI+III in skeletal muscle mitochondria (*A* and *B*) and in muscle homogenates (*C* and *D*) of wild-type and PGC-1α animals at different ages ($n = 6$ for each group, and bars represent SD). *, $P < 0.05$, **, $P < 0.001$. (E) Relative expression of PGC-1α and its targets NRF1 and TFAM in 3- and 22-month-old wild-type and PGC-1α animals ($n = 3$ for each group, and bars represent SD). (*F*) Western blot of DAP3 (small mitoribosomal subunit) and VDAC1 of skeletal muscle mitochondria of in 3- and 22-month-old wild-type and PGC-1α animals.

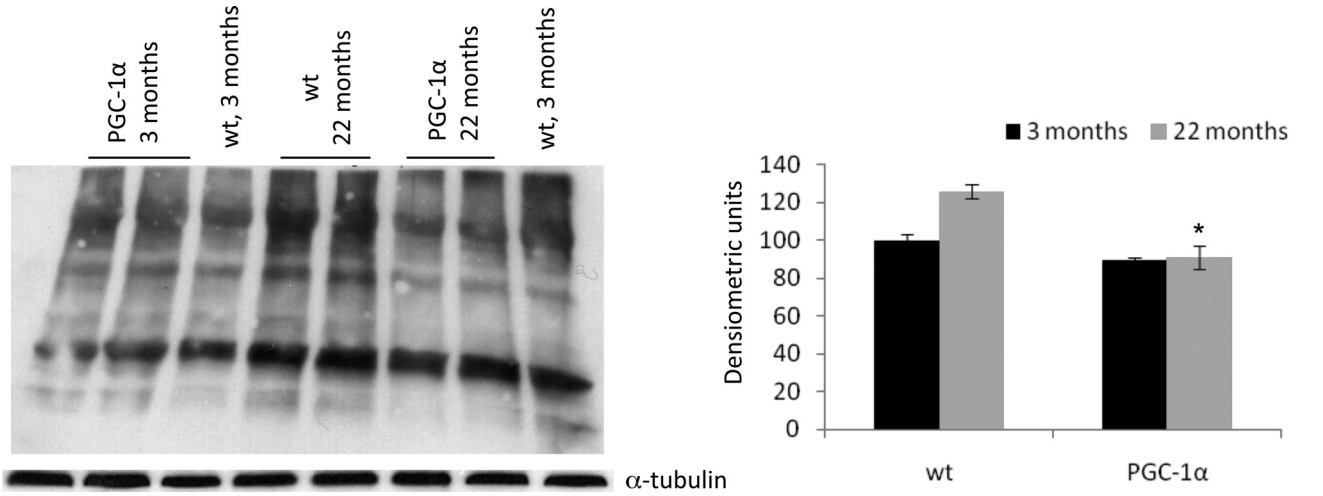

Fig. S3. Reduced protein oxidation in aged muscle with increased PGC-1α. Oxyblot analysis for 3- and 22-month-old wild-type and PGC-1α animals ($n = 6$ for each group, and bars represent SD). *, $P < 0.05$.

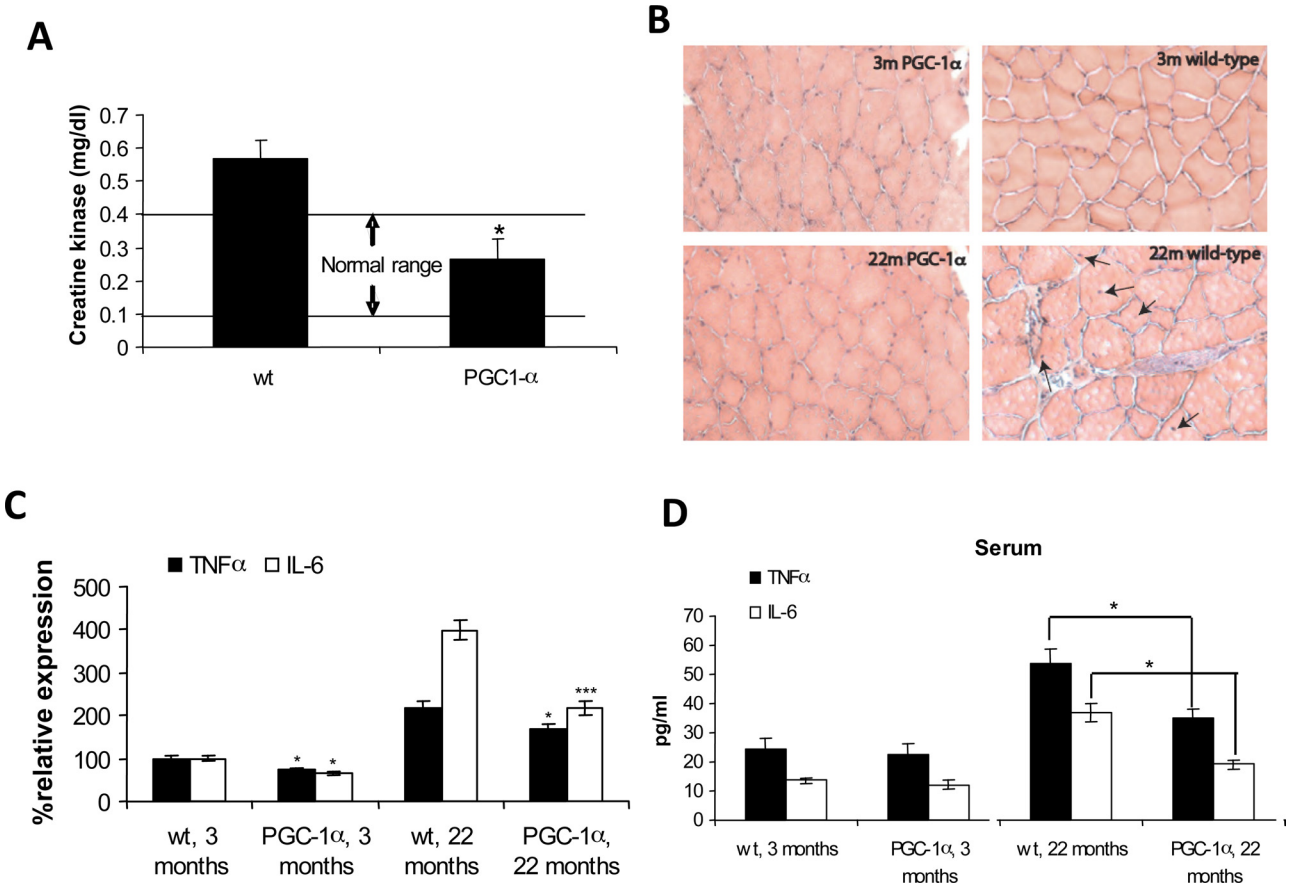

Fig. S4. Muscle damage and inflammatory cytokines are reduced in mice with increased PGC-1α in muscle. (*A*) Levels of circulating serum muscle creatine kinase for 22-month-old wild-type and PGC-1α animals ($n = 6$ for each group, and bars represent SD). *, $P < 0.001$. (*B*) H&E staining of biceps femoris from 3- and 22-month-old wild-type and PGC-1α animals. Arrows indicate fibers with centered nuclei. (*C*) Relative expression of TNFα and IL-6 in 3- and 22-month-old wild-type and PGC-1α animals ($n = 3$ for each group, and bars represent SD). *, $P < 0.05$, **, $P < 0.005$. (D) Levels of circulating inflammatory markers for 3- and 22-month-old wild-type and PGC-1α animals ($n = 6$ for each group, and bars represent SD). *, $P < 0.001$.

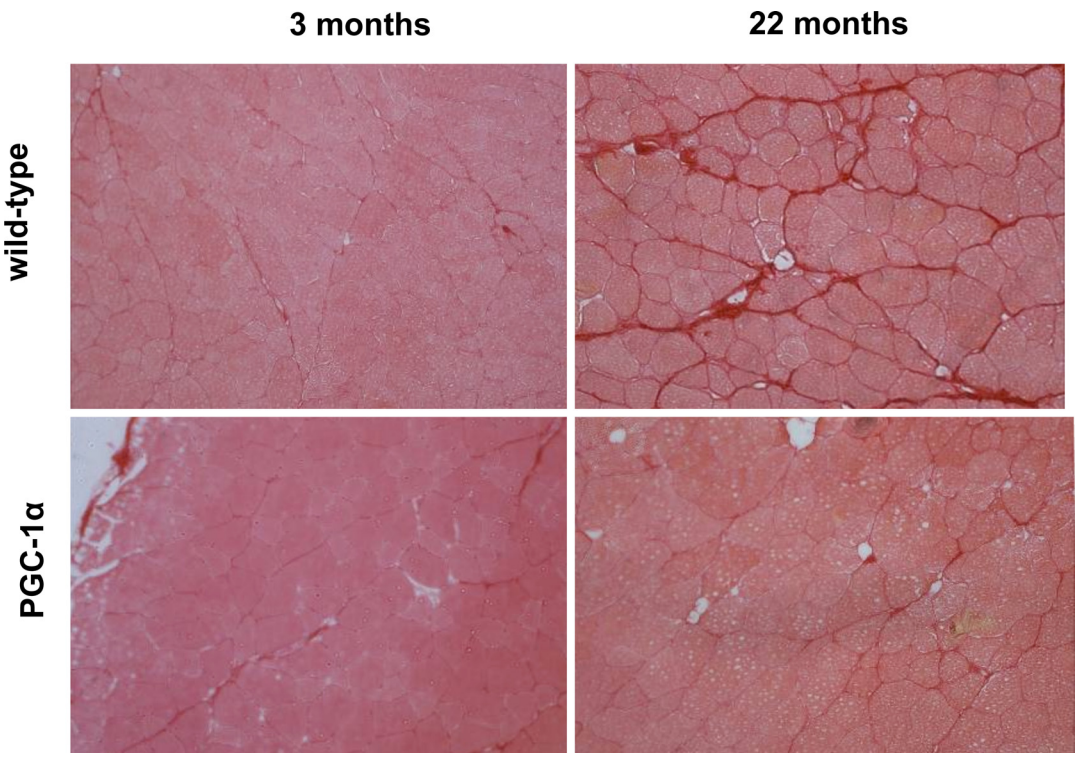

Fig. S5. Decreased connective tissue in aged muscle expressing PGC-1α. Picrosirus red staining of biceps femoris from 3- and 22-month-old wild-type and PGC-1α animals.

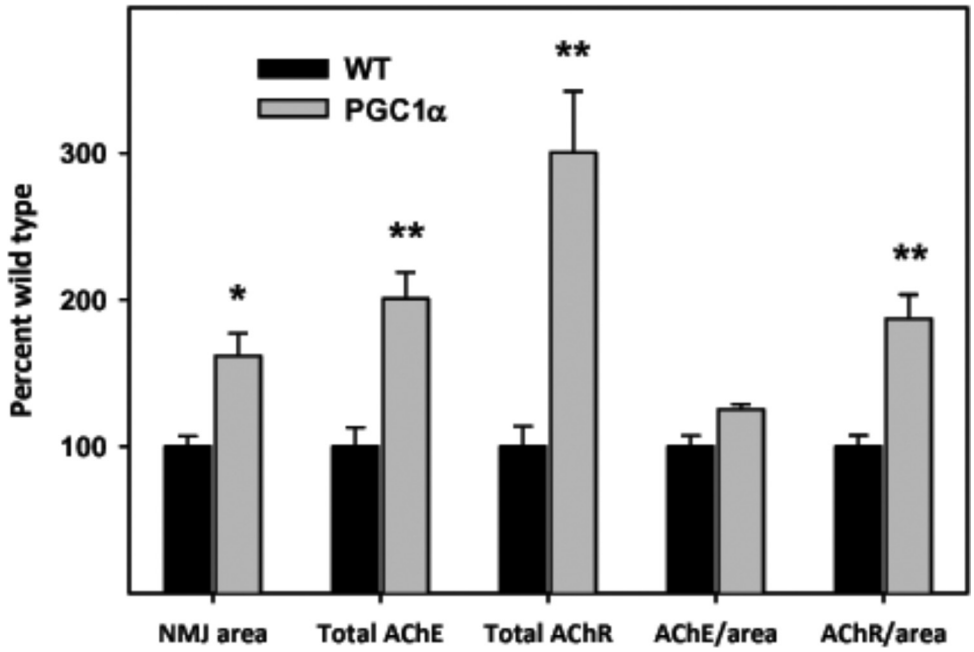

Fig. S6. Increased NMJ density in PGC-1α-expressing muscle. Quantification of NMJ sizes and relative AChE and AChR levels in 22-month-old wild-type and PGC-1α animals *, $P < 0.05$, **, $P < 0.005$.

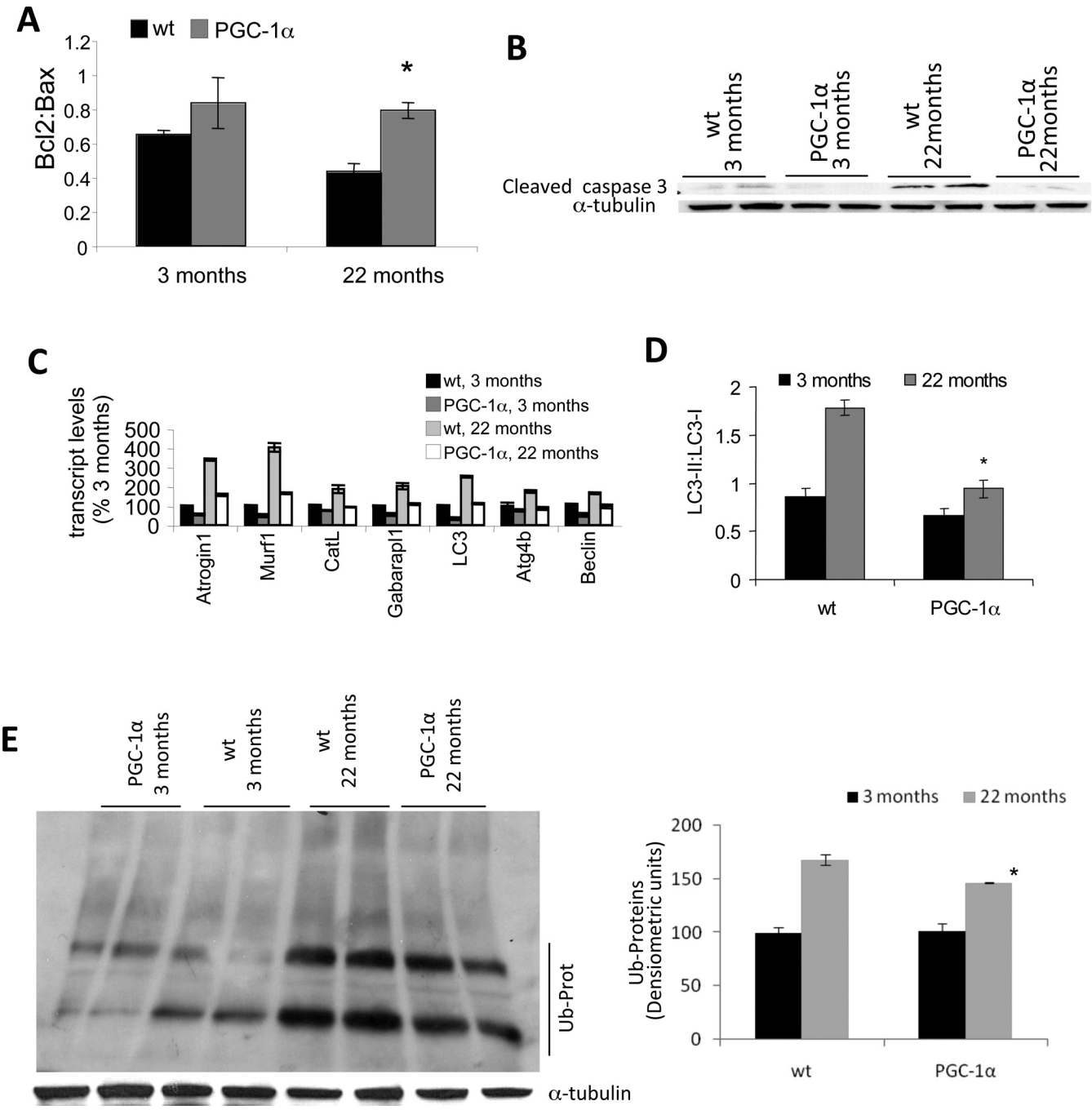

Fig. S7. Decreased muscle degradative pathways in mice expressing PGC-1α. (*A*) Quantification of Bax and Bcl-2 in skeletal muscle homogenates of 3- and 22-month-old mice ($n = 6$ for each group, and bars represent SD). *, $P < 0.01$. (*B*) Western blot of cleaved caspase 3 in skeletal muscle homogenates of in 3- and 22-month-old wild-type and PGC-1α animals. (*C*) Relative RNA levels of ubiquitin ligases (atrogin1, Murf1) and autophagy-related proteins (CatL, Gabarapl1, LC3, Atg4b, Beclin) in skeletal muscle from 3- and 22-month-old mice as determined by qRT-PCR ($n = 3$ for each group, and bars represent SD). (*D*) Quantification of LC3-I and LC3-II in skeletal muscle homogenates of 3- and 22-month-old mice ($n = 6$ for each group, and bars represent SD). *, $P < 0.01$. (E) Western blot of ubiquitin for 3- and 22-month-old wild-type and PGC-1α animals ($n = 6$ for each group, and bars represent SD). *, $P < 0.05$.

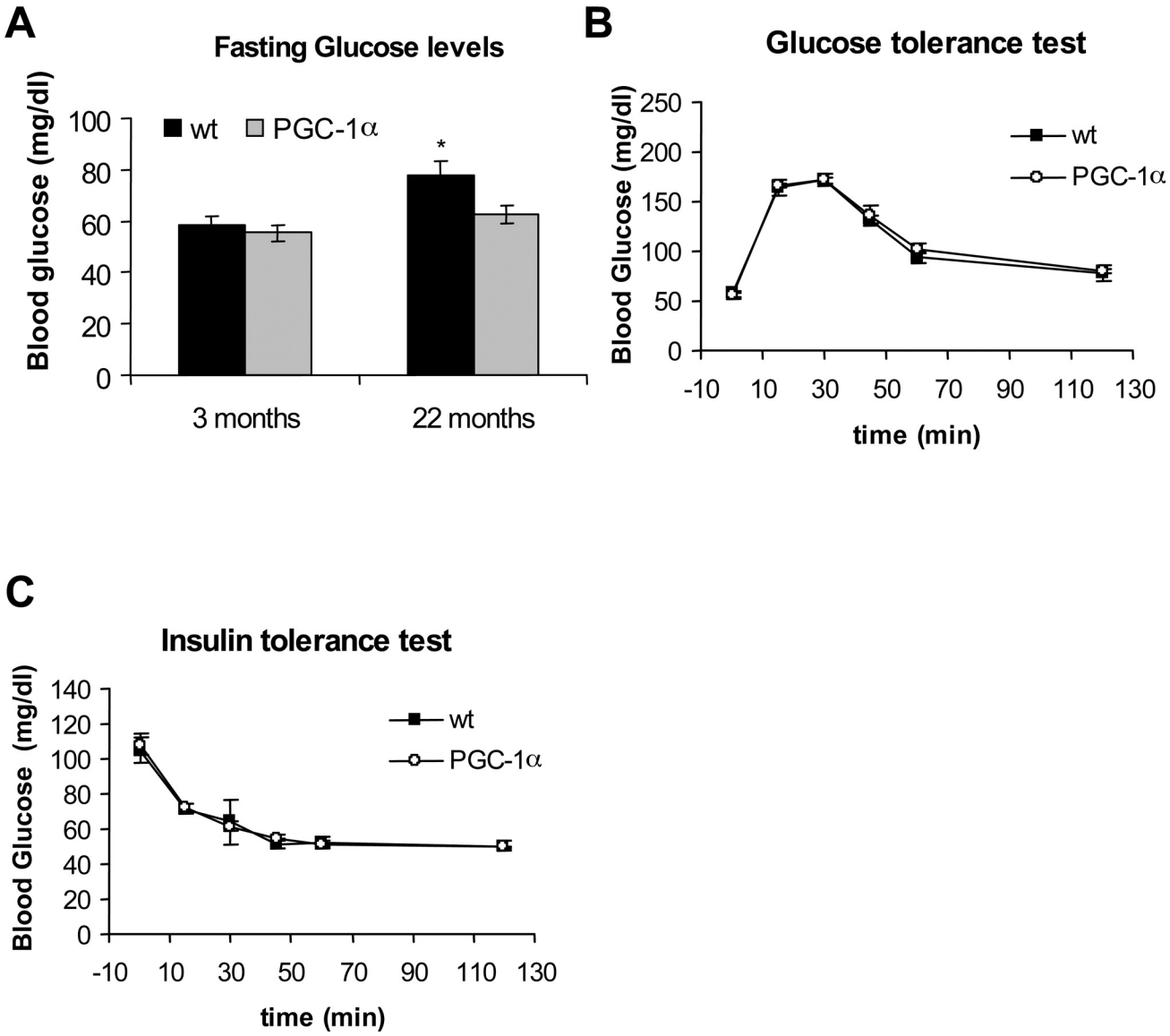

Fig. S8. Older mice with increased muscle PGC-1α have higher fasting glucose levels. (*A*) Fasting blood glucose levels ($n = 3$ for each group, and bars represent SD). (*B*) Glucose tolerance test in 3-month-old wild-type and MCK-PGC-1α animals ($n = 3$ for each group, and bars represent SD). (*C*) Insulin tolerance test in 3-month-old animals ($n = 3$ for each group, and bars represent SD).

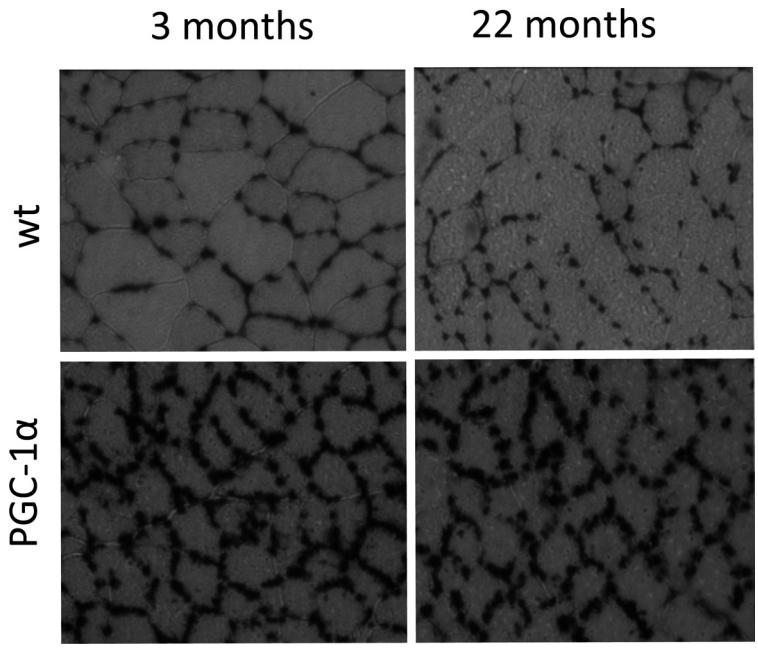

Fig. S9. Increased vascularization in PGC-1α-expressing muscle. Alkaline phosphatase staining of vascular network in biceps femoris of 3- and 22-month-old mice.